Analytical Investigation into the S-Parameters of Metamaterial Layers

Mohsen K. Meybodi* and **Kian Paran**

Abstract—Making use of mode matching method, a theoretical analysis of a metamaterial layer is presented. The unit cell of the structure is modeled by a TEM waveguide, and the metamaterial element is supposed as a discontinuity in the waveguide. Analyzing the structure using this model, mathematical relations between s-parameters of a metasurface are extracted. It is evident that the variation of each s-parameter is limited to an arc of circle on Smith chart. The key factors determining the location of each circle on plane are specified. Moreover, a discussion on the role of metasurface element in the determination of s-parameters of the structure is given. The variations of scattering transfer parameters on the plane are determined, too. The steps needed to derive these relations are described. Using these relations, simple and straightforward formulas are devised which can be used to predict the response of the metasurface. Finally, some metasurfaces will be analyzed by full-wave method. The new relations are well-agreed with simulation results.

1. INTRODUCTION

The advent and extension of metamaterial structures are one of the turning points in physics. The new strange behaviors of these structures, which do not happen or less happen to available structures, open new windows for the designers. Structure with near-zero or less than one refractive index, new waveguide structures, controllable surfaces, angular-independent surfaces, impedance-matching surfaces, thin absorbers, structures with ability to cloak an object, plasmonic nanowire, Negative Refractive Index (NRI) transmission lines, THz switches, THz imaging, molecular sensing are some of the evolutions occurring due to metamaterials in electromagnetics [1–10]. These structures help engineers and investigators to design new devices and improve the operation of prevalent systems.

An arrangement of many similar microstructures in the form of three dimensional periodic network creates a metamaterial structure [1–4]. In some cases, this arrangement happens in two dimensions. In reality, they create a layer of metamaterial, which is called metasurface. Existence of metamaterial elements increases the ability of structure to polarize electrically and magnetically. This effect can be different from one direction to another. It can result in creating anisotropic medium. Some methods are developed to determine the effective parameters of these structures, such as Nicolson-Ross-Weir (NRW) and Generalized Sheet Transition Condition (GSTC) [2, 11–13].

Analysis of metamaterials and metasurfaces is a crucial part of papers and books published in the context of metamaterials. This analysis can also be found in the subcategory of the study of periodic structures. For periodically-repeating environment, it is sufficient to simulate a period of structure in a specific box with suitable boundary conditions in sidewalls.

Reference [14] is one of the valuable publications about periodic structures. In [14], Marcuvitz analyzed a metal-strip grating in two polarizations. He studied the behavior of these structures and

presented relations for the equivalent admittance for each polarization. This work was continued by Ulrich in Far Infrared frequencies (FIR) [15]. The supposed structure was a thin metal mesh or grid which is embedded in free space. Ulrich found that the locus of reflection coefficient is an arc of a circle in complex reflection coefficient plane. For this derivation, he simultaneously considered two equalities; equality between total amplitude of propagating waves in both sides of the structure, and a relation between reflection and transmission coefficients of structure because of its passivity. A relation between phases of reflection and transmission coefficients versus amplitude of reflection coefficient was also found by him.

Focusing on metasurface, more discussions about mode matching technique would be carried on in the next section. TEM waveguide modeling helps to extract a simple equivalent circuit for metasurface. It is continued by extracting the variation of reflection coefficient for a typical metasurfaces located in the boundary of each two media. The locus of this variation is coincided with an arc of circle on the Smith chart. The parameters which are effective in determining the center and radius of this circle are given. Then, the role metasurface element in determining the reflection coefficient is described. After that, the variation of reflection coefficient versus frequency is considered. In the next step, all the remaining scattering parameters are obtained in terms of one of the scattering parameters. Variations of scattering transfer parameters (chain scattering parameters) in plane are determined, as well. In the third section, for some metasurfaces, the locus of reflection coefficient is extracted and could be accommodated by the relations derived in previous section. It is compared by simulation results of commercial software package. Finally, the summary of this discussion is mentioned in the conclusion.

2. MODAL ANALYSIS OF METASURFACE

As previously mentioned, the analysis of metasurface structure is reduced to the analysis of a unit cell surrounded with suitable boundary conditions in sidewalls. This modeling is called TEM waveguide [16] (Figure 1(b)). This model is simulated by different numerical methods, such as FDTD [17] and mode matching technique [18–21], to get the scattering parameters of the main structure.
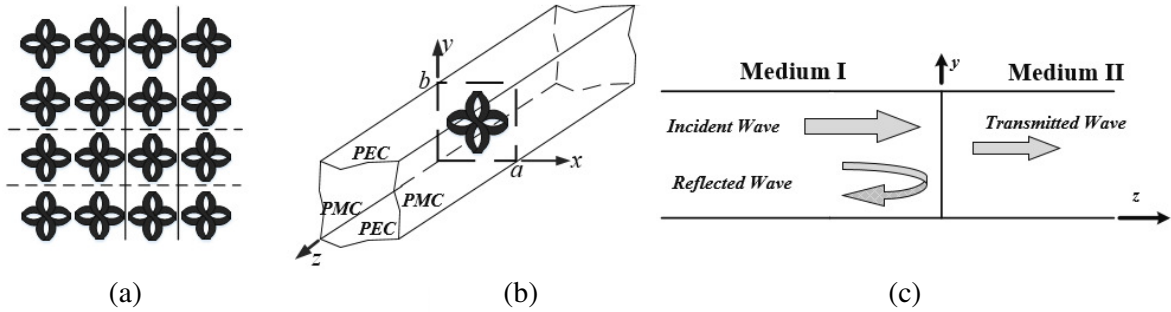

(a)	(b)	(c)

Figure 1. (a) Front view of a metasurface, (b) a unit cell of metasurface structure in the TEM waveguide, and (c) profile of the hypothesis waveguide with incident, reflected and transmitted waves.

Using the TEM waveguide modeling shows that a metasurface element has the role of a transverse discontinuity in hypothesis waveguide [18]. The existence of a discontinuity in the waveguide perturbs the flow of power. In this situation, some part of the incident power reflects back and forms the reflected wave, and the remaining power passes through metasurface plane, and forming the transmitted wave. The plane, which is coplanar with metasurface element, divides the inner medium of the waveguide into two media (Figure 1(c)), and it is called metasurface plane.

Based on modal analysis, each wave in the waveguide can be expanded in terms of different modes. In order to determine coefficient of each mode in this expansion, the boundary conditions in both sides of metasurface plane must be applied [22–27].

2.1. Mode Matching Technique

For using mode matching technique, all modes supported by the waveguide must be determined first. The TEM waveguide supports all TEM, TE and TM modes. The transverse component of electromagnetic fields for these modes are as follows [16–21].

$$
\text{TTEM}: \begin{cases} E_x = 0 & H_x = \dfrac{-E_y}{\eta_0} \\ E_y = A_{00} & H_y = 0 \end{cases}, \quad \text{TM}: \begin{cases} (E_x)_{mn} = \dfrac{m\pi}{a} a_{mn}\varphi_{mn}(x,y), \ (H_x)_{mn} = \dfrac{-(E_y)_{mn}}{Z_{mn}^{\text{TM}}} \\ (E_y)_{mn} = -\dfrac{n\pi}{b} a_{mn}\psi_{mn}(x,y), \ (H_y)_{mn} = \dfrac{(E_x)_{mn}}{Z_{mn}^{\text{TM}}} \end{cases}
$$

$$
\text{TE}: \begin{cases} (E_x)_{mn} = \dfrac{n\pi}{b} b_{mn}\varphi_{mn}(x,y), \ (H_x)_{mn} = \dfrac{-(E_y)_{mn}}{Z_{mn}^{\text{TE}}} \\ (E_y)_{mn} = \dfrac{m\pi}{a} b_{mn}\psi_{mn}(x,y), \ (H_y)_{mn} = \dfrac{(E_x)_{mn}}{Z_{mn}^{\text{TE}}} \end{cases}, \quad \begin{cases} \varphi_{mn}(x,y) \triangleq \sin\left(m\dfrac{\pi}{a}x\right)\sin\left(n\dfrac{\pi}{b}y\right) \\ \psi_{mn}(x,y) \triangleq \cos\left(m\dfrac{\pi}{a}x\right)\cos\left(n\dfrac{\pi}{b}y\right) \end{cases}
$$

$$(1)$$

where m and n indicate spatial variations of each mode in x and y directions, respectively. These modes are taken for intended waveguide (Figure 1(b)) without any discontinuity in it. Note that these modes make a set of orthogonal functions. The next step in using mode matching is to apply boundary conditions in both sides of metasurface plane. The necessary boundary conditions that must be satisfied are [24];

$$
\left(\vec{E}^i + \vec{E}^r\right)_t = \begin{cases} \left(\vec{E}^t\right)_t & R_m^c \\ 0 & R_m \end{cases}, \quad \hat{a}_z \times \left(\vec{H}^i + \vec{H}^r\right) = \begin{cases} \hat{a}_z \times \vec{H}^t & R_m^c \\ \vec{J}_- & R_m \end{cases} \tag{2}
$$

where $\vec{E}^i$, $\vec{E}^r$, $\vec{E}^t$, $\vec{H}^i$, $\vec{H}^r$ and $\vec{H}^t$ are incident, reflected and transmitted electric and magnetic fields, respectively. R_m is the part of unit cell that is covered by metal (and comprises metasurface element). The remaining hollow part of unit cell creates an aperture which is indicated here by R_m^c. The first relation in (2) implies that transverse components of electric field are zero on R_m, and are continuous on aperture R_m^c. Continuity of transverse magnetic fields on aperture is expressed by the second relation in (2).

As previously mentioned, impinging a wave on discontinuity leads to exciting higher order modes in waveguide. These modes form reflected and transmitted waves. Therefore, each reflected and transmitted wave is expressed by a linear combination of different modes. If the incident wave is a TEM wave with amplitude A_{00}, then incident, reflected and transmitted waves are;

$$
\begin{cases} \vec{E}^i = \hat{a}_y \left(A_{00} e^{-j\beta_{00}z}\right) \\[4pt] \vec{E}^r = \hat{a}_x \displaystyle\sum_{k=\text{TM,TE}}\sum_{m,n} (E_x^r)_{mn}^k e^{j\beta_{mn}z} + \hat{a}_y \left(a_{00} e^{j\beta_{00}z} + \displaystyle\sum_{k=\text{TM,TE}}\sum_{m,n} (E_y^r)_{mn}^k e^{j\beta_{mn}z}\right) + \hat{a}_z E_z^r \\[4pt] \vec{E}^t = \hat{a}_x \displaystyle\sum_{k=\text{TM,TE}}\sum_{m,n} (E_x^t)_{mn}^k e^{j\beta_{mn}z} + \hat{a}_y \left(c_{00} e^{j\beta_{00}z} + \displaystyle\sum_{k=\text{TM,TE}}\sum_{m,n} (E_y^t)_{mn}^k e^{j\beta_{mn}z}\right) + \hat{a}_z E_z^t \end{cases}
$$

$$
\begin{cases} \vec{H}^i = \hat{a}_x \left(\dfrac{-A_{00}}{\eta_0} e^{-j\beta_{00}z}\right) \\[4pt] \vec{H}^r = \hat{a}_x \left(\dfrac{a_{00}}{\eta_0} e^{j\beta_{00}z} + \displaystyle\sum_{k=\text{TM,TE}}\sum_{m,n} \dfrac{(E_y^r)_{mn}^k}{Z_{mn}^k} e^{j\beta_{mn}z}\right) - \hat{a}_y \displaystyle\sum_{k=\text{TM,TE}}\sum_{m,n} \dfrac{(E_x^r)_{mn}^k}{Z_{mn}^k} e^{j\beta_{mn}z} + \hat{a}_z H_z^r \\[4pt] \vec{H}^t = \hat{a}_x \left(-\dfrac{c_{00}}{\eta_0} e^{-j\beta_{00}z} - \displaystyle\sum_{k=\text{TM,TE}}\sum_{m,n} \dfrac{(E_y^t)_{mn}^k}{Z_{mn}^k} e^{-j\beta_{mn}z}\right) + \hat{a}_y \displaystyle\sum_{k=\text{TM,TE}}\sum_{m,n} \dfrac{(E_x^t)_{mn}^k}{Z_{mn}^k} e^{-j\beta_{mn}z} + \hat{a}_z H_z^r \end{cases}
$$

$$
\beta_{mn} = \sqrt{\varepsilon_r \varepsilon_0 \mu_0 \omega^2 - \left(\dfrac{m\pi}{a}\right)^2 - \left(\dfrac{n\pi}{b}\right)^2}, \quad Z_{mn}^{\text{TE}} = \dfrac{\omega\mu_0}{\beta_{mn}}, \quad Z_{mn}^{\text{TM}} = \dfrac{\beta_{mn}}{\omega\varepsilon_r\varepsilon_0}
$$

$$(3)$$

where A_{00}, a_{00}, c_{00} are the amplitudes of incident, reflected and transmitted waves for TEM mode. β_{mn} is propagation constant, and η_0, Z_{mn}^{TE} and Z_{mn}^{TM} are characteristic impedance for TEM, TE and TM modes, respectively. All β_{mn}, η_0, Z_{mn}^{TE} and Z_{mn}^{TM} in reflected and transmitted waves are related to mediums I and II, respectively. The above relations are achieved with supposing that two media are extended into infinity.

For calculating all coefficients based on mode matching technique, each of electric and magnetic fields in Eq. (2) is substituted by expansions of incident, reflected and transmitted waves. This substitution changes the domain from spatial into modal domain (spectral domain). In the modal domain, we are faced with a system of linear algebraic equations. Computing all reflected and transmitted coefficients depends on the solution of this system.

It should be noted that similar expression about electric field in Eq. (2) exists about transverse electric fields in medium II. The transverse components of electric field are zero on R_m and are continuous on aperture (R_m^c).

$$\left(\vec{E}^t\right)_t = \left\{ \begin{array}{ll} \left(\vec{E}^i + \vec{E}^r\right)_t, & R_m^c \\ 0 = \left(\vec{E}^i + \vec{E}^r\right)_t, & R_m \end{array} \right. = \left(\vec{E}^i + \vec{E}^r\right)_t \rightarrow \left\{ \begin{array}{l} c_{mn} = a_{mn} + A_{00}\delta_{0m}\delta_{0n} \\ d_{mn} = b_{mn} \end{array} \right. \quad m,n = 0,1,2,\ldots \quad (4)$$

The first relation in Eq. (4) means that there are no variations in the tangential component of electric field through metasurface plane. Simultaneously considering this note with the modal expansions of electric fields in Eq. (3) results in equality of total amplitude of each mode in both sides of element in Eq. (4) (see Appendix A). Same as this analysis is used in [28, 29]. In [28], the authors propose a wide-band equivalent circuit for a 2D array of scatterers with the aid of modal analysis. Also, this analysis is used to illustrate the behavior of a 2D array of Split Ring Resonators (SRRs) in [29].

2.2. The Variations of S-parameters on Smith Chart

Considering Eq. (4) versus $m = n = 0$, it is possible to extract a relation between the reflection and transmission coefficients of the structure;

$$s_{11} = \frac{a_{00}/\sqrt{(\eta_0)_{\text{I}}}}{A_{00}/\sqrt{(\eta_0)_{\text{I}}}}, \quad s_{21} = \frac{c_{00}/\sqrt{(\eta_0)_{\text{II}}}}{A_{00}/\sqrt{(\eta_0)_{\text{I}}}} = \sqrt{\frac{(\eta_0)_{\text{I}}}{(\eta_0)_{\text{II}}}}\left(1 + s_{11}\right) \quad (5)$$

Repeating the last relation for a wave impinging on metasurface element in medium II, we have,

$$s_{12} = \sqrt{\frac{(\eta_0)_{\text{II}}}{(\eta_0)_{\text{I}}}}\left(1 + s_{22}\right) = s_{21} \quad (6)$$

where the equality between s_{12} and s_{21} is a result of reciprocity. Simultaneously considering Eqs. (5) and (6) directs us into Eq. (7),

$$s_{12} = s_{21} \rightarrow \sqrt{\frac{(\eta_0)_{\text{I}}}{(\eta_0)_{\text{II}}}}\left(1 + s_{11}\right) = \sqrt{\frac{(\eta_0)_{\text{II}}}{(\eta_0)_{\text{I}}}}\left(1 + s_{22}\right) \rightarrow s_{22} = \frac{(\eta_0)_{\text{I}}}{(\eta_0)_{\text{II}}}\left(1 + s_{11}\right) - 1 \quad (7)$$

If the TEM waveguide with metasurface element in middle is supposed in form of a two-port network, the calculated parameters in above form the elements of the scattering matrix of this network (S). Equations (5), (6) and (7) imply that all s-parameters of a typical metasurface are determined in terms of one of them (here s_{11}).

Since metasurface is a passive structure, then;

$$SS^* = I \rightarrow \left\{ \begin{array}{l} |s_{11}|^2 + s_{12}s_{21}^* = 1 \\ s_{11}s_{12}^* + s_{12}s_{22}^* = 0 \end{array} \right. \rightarrow \left\{ \text{Re}\left(s_{11}\right) + \frac{(\eta_0)_{\text{I}}}{(\eta_0)_{\text{II}} + (\eta_0)_{\text{I}}} \right\}^2 + \left\{\text{Im}\left(s_{11}\right)\right\}^2 = \left(\frac{(\eta_0)_{\text{II}}}{(\eta_0)_{\text{II}} + (\eta_0)_{\text{I}}}\right)^2 \quad (8)$$

The steps needed to derive Eq. (8) are expressed in Appendix B. The relation (8) is a circle on complex reflection coefficient plane (Smith chart). The center and radius of this circle are $(-(\eta_0)_{\text{I}}/[(\eta_0)_{\text{II}} + (\eta_0)_{\text{I}}], 0)$ and $(\eta_0)_{\text{II}}/[(\eta_0)_{\text{II}} + (\eta_0)_{\text{I}}]$, respectively. This circle crosses horizontal line $\{\text{Re}(s_{11})\}$ in two points $(-1, 0)$ and $([(\eta_0)_{\text{II}} - (\eta_0)_{\text{I}}]/[(\eta_0)_{\text{II}} + (\eta_0)_{\text{I}}], 0)$. The point $(-1, 0)$ is corresponding

to when the metasurface element completely covers the unit cell. When no element exists on the boundary of two media, the return loss is equal to $[(\eta_0)_{\mathrm{II}} - (\eta_0)_{\mathrm{I}}/[(\eta_0)_{\mathrm{II}} + (\eta_0)_{\mathrm{I}}]$ (second point).

Regardless of geometrical characteristics of metasurface element, the other s-parameters of metasurface are located in specific circles, which are dependent on electromagnetic properties in both sides of metasurface. The circles corresponding to s_{21} and s_{22} are;

$$
\left\{ \mathrm{Re}\left(s_{21}\right) - \frac{\sqrt{(\eta_0)_{\mathrm{I}}(\eta_0)_{\mathrm{II}}}}{(\eta_0)_{\mathrm{II}} + (\eta_0)_{\mathrm{I}}} \right\}^2 + \left\{ \mathrm{Im}\left(s_{21}\right) \right\}^2 = \left(\frac{(\eta_0)_{\mathrm{I}}(\eta_0)_{\mathrm{II}}}{((\eta_0)_{\mathrm{II}} + (\eta_0)_{\mathrm{I}})^2} \right)
$$

$$
\left\{ \mathrm{Re}\left(s_{22}\right) + \frac{(\eta_0)_{\mathrm{II}}}{(\eta_0)_{\mathrm{II}} + (\eta_0)_{\mathrm{I}}} \right\}^2 + \left\{ \mathrm{Im}\left(s_{22}\right) \right\}^2 = \left(\frac{(\eta_0)_{\mathrm{I}}}{(\eta_0)_{\mathrm{II}} + (\eta_0)_{\mathrm{I}}} \right)^2
$$

(9)

Note that the circles s_{11} and s_{22} cross each other at least once. This common point is $(-1, 0)$. This point is corresponding to where a metal plate is sandwiched between two media. For metamaterial structure, it happens when metamaterial element totally covers unit cell. Since the variation of each s-parameter is on a circle, it is expected that the real and imaginary parts of each parameters are expressed in terms of absolute value of that parameter. This is discussed in the following.

2.3. The Effect of Metasurface Element on the Scattering Parameters

The parameter s_{11} in above relations can be rewritten in terms of center and radius of circle;

$$
s_{11} = a_1 + r_1 e^{j\theta}, \quad a_1 = \frac{-(\eta_0)_{\mathrm{I}}}{(\eta_0)_{\mathrm{II}} + (\eta_0)_{\mathrm{I}}}, \quad r_1 = \frac{(\eta_0)_{\mathrm{II}}}{(\eta_0)_{\mathrm{II}} + (\eta_0)_{\mathrm{I}}}, \quad r_1 = 1 + a_1
$$

$$
s_{21} = \sqrt{\frac{(\eta_0)_{\mathrm{I}}}{(\eta_0)_{\mathrm{II}}}} r_1 \left(1 + e^{j\theta} \right), \quad s_{22} = \frac{(\eta_0)_{\mathrm{I}}}{(\eta_0)_{\mathrm{II}}} r_1 \left(1 + e^{j\theta} \right) - 1
$$

(10)

These relations separate the role of metasurface element from the effect of electromagnetic properties of two media as well. As seen in Eq. (10), the center and radius of each circle depend only on electromagnetic properties of two media. The geometrical properties of element (shape and size) have no effect on determining them. The effect of metamaterial element reflects on the parameter θ. Two media, surrounded the unit cell, are effective in determining the parameter θ, too. Comparing these two factors, it could be said that the metasurface element has the main role in determining θ, and the effect of surrounded media is weaker. In brief, the surrounded media determine the circle, and geometrical specifications of the element determine the situation of s_{11} on the circle. With this notation, determinant of the scattering matrix (S) is $-e^{j\theta}$.

2.4. The Variations of Real and Imaginary Parts of Reflection Coefficient

Here, we apply the principle of conservation of complex power about metasurface element in TEM waveguide model. According to this principle, the summation of complex power incident on discontinuity from two media is zero in Eq. (11).

$$
\int_S \left[\left(\vec{E}^{\mathrm{I}} \right)_t \times \left(\vec{H}^{\mathrm{I}} \right)_t^* \right] \cdot \hat{a}_z ds + \int_S \left[\left(\vec{E}^{\mathrm{II}} \right)_t \times \left(\vec{H}^{\mathrm{II}} \right)_t^* \right] \cdot (-\hat{a}_z) ds = 0
$$

$$
\rightarrow \int_S \left\{ \left(\vec{E}^{\mathrm{I}} \right)_t \times \left[\left(\vec{H}^{\mathrm{I}} \right) - \left(\vec{H}^{\mathrm{II}} \right) \right]_t^* \right\} \cdot \hat{a}_z ds = 0 \rightarrow \int_S \left[\left(\vec{E}^i + \vec{E}^r \right)_t \times \left(\vec{H}^i + \vec{H}^r - \vec{H}^t \right)_t^* \right] \cdot \hat{a}_z ds = 0
$$

(11)

All functions in Eq. (11) are integrated over the surface of unit cell. The continuity of tangential component of electric fields through discontinuity in Eq. (4) is used to simplify the above relation.

Impinging a TEM wave with parallel polarization on the metal-strip grating which is embedded in air, leads to excite TEM and TE modes in reflected and transmitted waves (Figure 2). By substituting

the expansions of all waves in the last relation of Eq. (11), it yields;

$$\int_S \left(A_0 + \sum_m a_m \cos\left(m\frac{\pi}{s}x\right) \right) \left(\sum_m \frac{2a_m}{Z_m^{\mathrm{TE}}} \cos\left(m\frac{\pi}{s}x\right) \right)^* dx = 0$$

$$\rightarrow 2\frac{|a_0|^2 + A_0(a_0)^*}{\eta_0} + \frac{|a_1|^2}{\left(Z_1^{\mathrm{TE}}\right)^*} + \frac{|a_2|^2}{\left(Z_2^{\mathrm{TE}}\right)^*} + \ldots = 0 \tag{12}$$

The second relation in Eq. (12) is obtainable by directly multiplying the boundary conditions in Eq. (2), too. In frequency range below of the first TE mode, all Z_m^{TE}s are imaginary. Separating the real and imaginary parts of last relation results into ($A_0 = 1$);

$$\mathrm{Re}\,(s_{11}) = -|s_{11}|^2 \rightarrow \mathrm{Im}\,(s_{11}) = \pm |s_{11}|\sqrt{1 - |s_{11}|^2}$$

$$\frac{|a_1|^2}{\left(Z_1^{\mathrm{TE}}\right)^*} + \frac{|a_2|^2}{\left(Z_2^{\mathrm{TE}}\right)^*} + \ldots = j2\frac{\mathrm{imag}\,(a_0)}{\eta_0} = sj2\frac{|a_0|\sqrt{1 - |a_0|^2}}{\eta_0} \tag{13}$$

About the imaginary part of s_{11}, the shape of element in the structure helps to select the sign. It will be described more in the next section. For this structure, the plus sign must be selected. These relations indicate that for any metasurface, it is possible to obtain the real and imaginary parts of s_{11} in terms of absolute value of s_{11} ($|s_{11}|$). When the metasurface is sandwiched between two different media, these relations must be modified (Appendix C). Same as these relations are derived by [15] for angles of s_{11} versus $|s_{11}|$. The last expression in Eq. (13) is a relation between total energy, stored around grating by excitation of higher order modes, and the imaginary part of dominant mode in reflected wave. Drawing the real and imaginary parts of s_{11} versus $|s_{11}|$ shows that with increasing $|s_{11}|$ from zero to one, $\mathrm{Re}(s_{11})$ uniformly decreases, while $\mathrm{Im}(s_{11})$ has an extremum in this range (at $\theta = 90$). This point is corresponding to when the excitation of higher order modes causes the highest stored energy around the structure.

2.5. Locus of Scattering Transfer Parameters on the Plane

The scattering transfer parameters of metasurface structure can be obtained in terms of s-parameters [30],

$$T_{11} = \frac{1}{s_{21}} = \frac{1}{\sqrt{(\eta_0)_{\mathrm{I}}/(\eta_0)_{\mathrm{II}}}\,(1 + s_{11})} = \frac{1}{\sqrt{(\eta_0)_{\mathrm{I}}/(\eta_0)_{\mathrm{II}}}\,r_1\,(1 + e^{j\theta})} \rightarrow T_{11} = \frac{1}{b_1\,(1 + e^{j\theta})},$$

$$b_1 = \sqrt{\frac{(\eta_0)_{\mathrm{I}} + (\eta_0)_{\mathrm{II}}}{(\eta_0)_{\mathrm{I}}(\eta_0)_{\mathrm{II}}}} \tag{14}$$

$$\begin{cases} T_{11} = \dfrac{1}{b_1\,(1 + e^{j\theta})} = \dfrac{1}{2b_1}\left(1 - j\tan\left(\dfrac{\theta}{2}\right)\right), & T_{21} = \dfrac{s_{11}}{s_{21}} = \dfrac{-1 + r_1\,(1 + e^{j\theta})}{b_1\,(1 + e^{j\theta})} = \dfrac{r_1}{b_1} - T_{11} \\[4mm] T_{12} = \dfrac{-s_{22}}{s_{21}} = \dfrac{r_1\,(1 + e^{j\theta}) - e^{j\theta}}{b_1\,(1 + e^{j\theta})} = T_{21}^*, & T_{22} = \dfrac{-\det(S)}{s_{21}} = \dfrac{e^{j\theta}}{s_{21}} = \dfrac{1}{b_1\,(1 + e^{-j\theta})} = T_{11}^* \end{cases}$$

As evident in Eq. (14), in the T_{11} plane $\{\mathrm{Re}(T_{11}) - \mathrm{Im}(T_{11})\}$, T_{11} is a part of straight line $\{\mathrm{Re}(T_{11}) = \mathrm{constant}\}$. The real part of T_{11} is constant while the imaginary part of T_{11} varies dominantly in terms of the specifications of element. The parameter T_{22} is symmetry of T_{11} about the $Re(T_{11})$-axis. The parameters T_{21} and T_{12} are a part of straight, too. These parameters comprise the elements of scattering transfer matrix (T). Determinant of this matrix is 1 for the metasurface structures.

2.6. Equivalent Circuit

The TEM waveguide model used to simulate structure, is useful for extracting equivalent circuit for metasurface (Figure 1(b)). Two transmission lines in equivalent circuit are representations of mediums
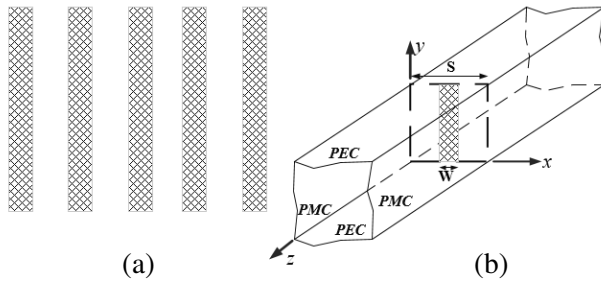
Figure 2. (a) A structure consisted of parallel strips, (b) a unit cell of structure.
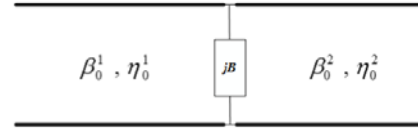

Figure 3. Equivalent circuit for metasurface structure.

I and II in TEM waveguide (Figure 3). According to TEM waveguide model, each of these transmission lines is an ideal parallel plate with width a and height b. Their characteristic impedances (η_0^1, η_0^2) and propagation constants (β_0^1, β_0^2) are characteristic impedances and propagation constants of TEM mode for mediums I and II. The length of each transmission line is equal to the length of waveguide.

While the dimensions of unit cell are smaller than wavelength of incident wave, all higher order modes, excited around the element, are evanescent. Excitation of these modes causes to store energy around discontinuity. No power is transferred into source or loaded by these modes. This storage is represented by a reactance or susceptance in equivalent circuit. Continuity of tangential components of electric fields in Eq. (3) indicates that the voltage is constant at the connection point of two transmission lines. Therefore, excitation of higher order modes appears in the form of a parallel susceptance in equivalent circuit [24]. This susceptance is a function of frequency, geometrical specifications of element, and electromagnetic properties of surrounded media. Figure 3 shows a simple equivalent circuit for metasurface structure. More exactly equivalent circuit is presented in [31–33].

With considering the equivalent circuit, input admittance, seen by medium I, is equal to parallel combination of the characteristic impedance of medium II and the susceptance of metasurface. It is consistent with what were obtained in the previous discussions. The circles s_{11} and s_{22} are accordant with constant-G circle of Smith chart. The characteristic impedance of transmission line determines the constant-G circle.
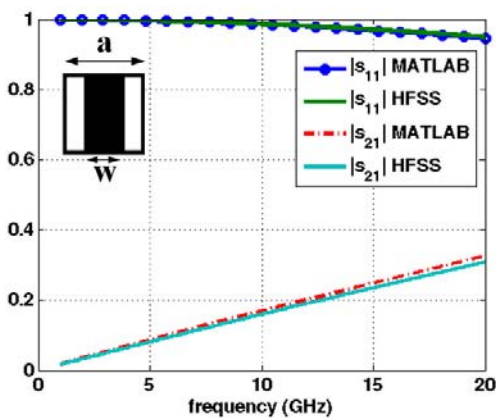

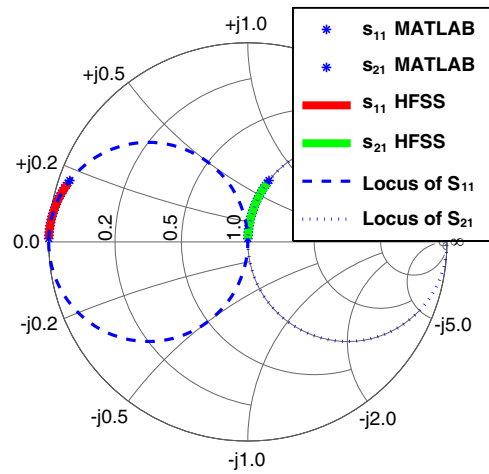**Figure 4.** The frequency variations of s_{11} and s_{21} for metal grating (parallel polarization).

Figure 5. The variations of s_{11} and s_{21} on the Smith chart.

3. SIMULATION RESULTS

In this section, several structures are analyzed using mode matching method. This method is implemented by MATLAB. To prove the validity of results and derived formulas, all simulations are repeated by HFSS. In the following simulations, it is supposed that two media are extended into infinity, and the reference planes located 10 mm away from discontinuity in both sides. For demonstrating the results on Smith chart, all parameters are calculated on the metasurface plane.

The first structure is a metallic strip grating illuminated by a wave which polarization is along the grating (Figure 2). A unit cell of this structure is shown in Figure 4. Table 1 specifies the geometrical characteristics of metasurface element. The frequency variations of reflection and transmission coefficients are plotted in Figure 4 for this structure. Figure 4 shows that the major part of incident power is reflected back in medium I. The frequency variations of s-parameters on Smith chart are demonstrated in Figure 5. The variations of s_{12} and s_{22} for this structure are the same as the variations of s_{21} and s_{11}, respectively. The dash lines on Figure 5 are drawn based on relations (8) and (9). The metallic strips in this structure behave in the same way as parallel inductance in equivalent circuit. Figure 6 displays the frequency variations of equivalent inductance for the metal grating with dimensions specified in Table 1. As seen, this equivalent inductance is approximately constant in intended frequency range.

Figure 7 shows the variations of reflection and transmission coefficients versus the width of strip for 10 GHz. According to Figure 7, the more the parameter w increases, the closer to -1 the parameter s_{11} moves. In the limit, when each strip covers all area of unit cell, s_{11} goes to -1. In general, with increasing the area of metasurface element, the parameters s_{11} and s_{22} move to -1 along the corresponding circles ($\theta \to \pi$ in Eq. (10)). Also, the parameters s_{21} and s_{12} move to origin ($\Gamma = 0$) along the corresponding circle (in counterclockwise direction). Note that with decreasing frequency, the parameter θ goes to π for this structure, so that when θ equals to π, the value of s_{11} is -1. It is predictable from the model used for simulating metasurface. If the frequency is zero, two conductors of ideal parallel plate in model are shorted by the strip. The variations of real and imaginary parts of s_{11} versus $|s_{11}|$ are shown in Figure 8 for this structure. Since this structure has the inductive properties, then $+$ sign for Im(s_{11}) is selected. Clearly seen, with increasing $|s_{11}|$ from zero to one, real part of s_{11} uniformly decreases, while

Table 1. Physical dimensions of grating structure for the first structure.

a	w	Medium I	Medium II
2.5 mm	0.5 mm	air	air

Table 2. Physical dimensions of grating for the second example.

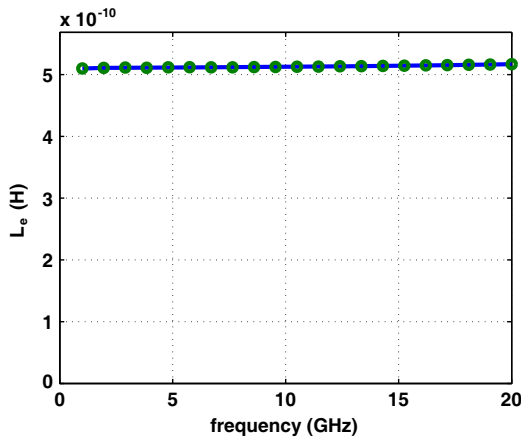| a	w	Medium I	medium II
2 mm	1.5 mm	air	Teflon

Figure 6. The variations of equivalent inductance versus frequency.
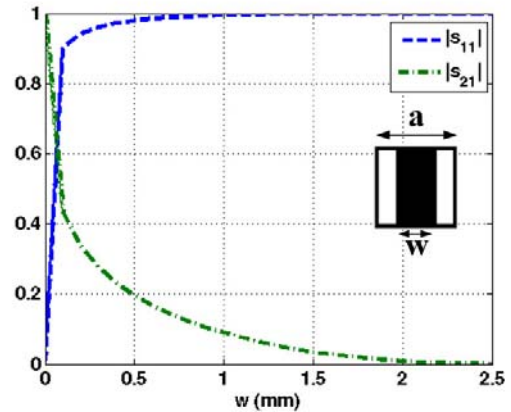

Figure 7. The variation of reflection coefficient versus the width of strip (10 GHz).

the graph of $\text{Im}(s_{11})$ has a maximum where $|s_{11}|$ is equal to $1/\sqrt{2}$ ($\theta = \pi/2$ in Eq. (10)). This point is corresponding to when the excitation of higher order modes causes the highest stored energy around the structure.

The second structure is metal grating printed on Teflon. In this example, the strips are perpendicular to polarization of incident wave (Figure 9). It causes to excite only TEM and TM modes around metasurface plane. Physical dimensions of this structure is available in Table 2. Simulation results for this structure are demonstrated in Figure 9. According to Figure 9, the major part of incident power is transmitted through medium II. Figure 10 displays the frequency variations of s-parameters on Smith chart for this structure. The scattering transfer parameters for this structure are shown in Figure 11. As previously discussed, these parameters are located along the straight line.

In contrast to the previous structure, metasurface element in this structure plays the role of parallel capacitance in equivalent circuit. The frequency variations of equivalent capacitance are shown in Figure 12. Figure 13 shows the real and imaginary parts of the reflection coefficient in terms of $|s_{11}|$. In contrast to what happened about the previous structure, the imaginary part of reflection coefficient is lower than zero, and it has a minimum. This point happens when the stored energy is maximum around metasurface. The variations of real part of reflection coefficient is similar to the previous structure. Same as the previous structure, the increment in w causes the parameters s_{11} and s_{22} to
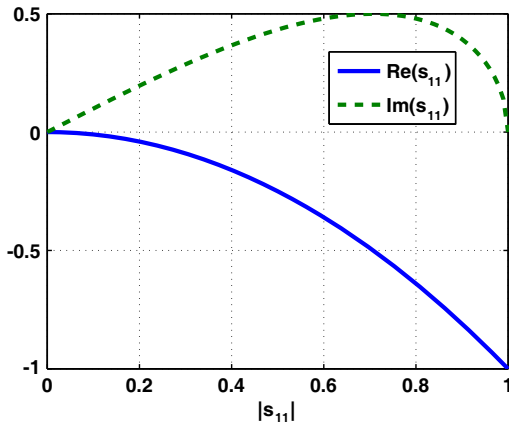

Figure 8. The variations of real and imaginary parts of s_{11} versus $|s_{11}|$.
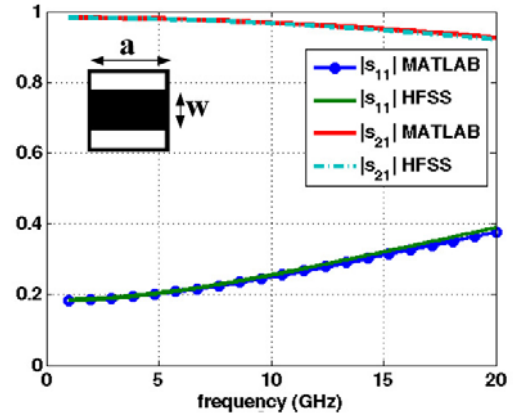

Figure 9. The variations of s_{11} and s_{21} of metal strips for perpendicular polarization.
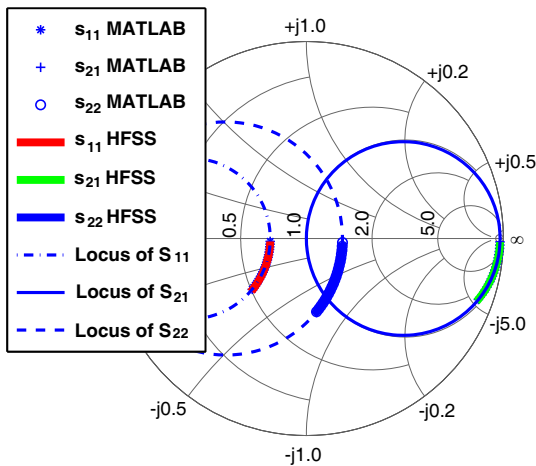

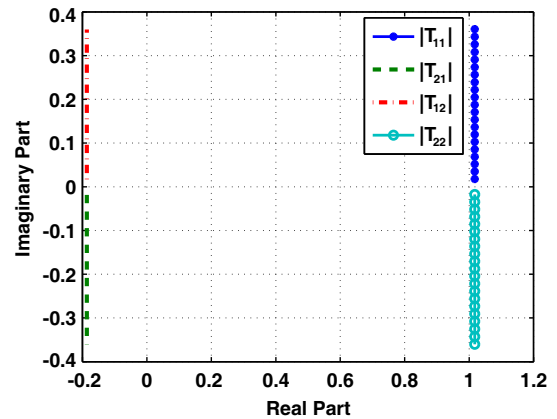**Figure 10.** The frequency variations of s_{11}, s_{21} and s_{22} on the Smith chart.

Figure 11. The variations of scattering transfer parameters on T-plane.

move to -1 along the corresponding circles. Decreasing and increasing frequency causes s_{11} to move to $((\eta_0)_{II} - (\eta_0)_I)/((\eta_0)_{II} + (\eta_0)_I)$ and -1, respectively.

The next example is a metasurface composed of square patches (Figure 14). Let metasurface elements be printed on FR4. Physical dimensions of each element are presented in Table 3. Figure 14 displays simulation results of this structure. As seen, more of the incident power is reflected with increasing frequency. The variations of the scattering parameters on Smith chart are presented in Figure 15. The variations of scattering transfer parameters are demonstrated in Figure 16 for this structure.

An array of square loops comprises the forth metasurface (Figure 17). Let metasurface elements are located in the boundary between air and FR4. Geometrical properties of each element are available in Table 4. Simulation results of this structure are presented in Figure 17. The variations of the scattering
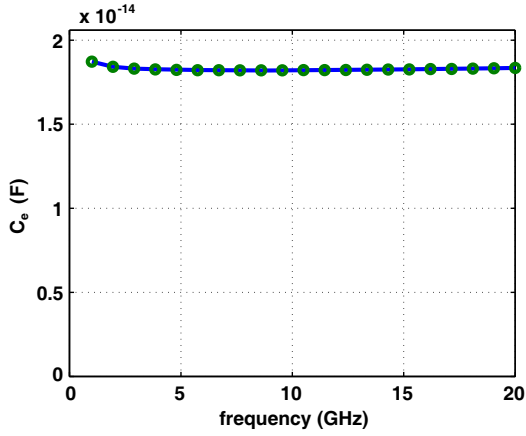

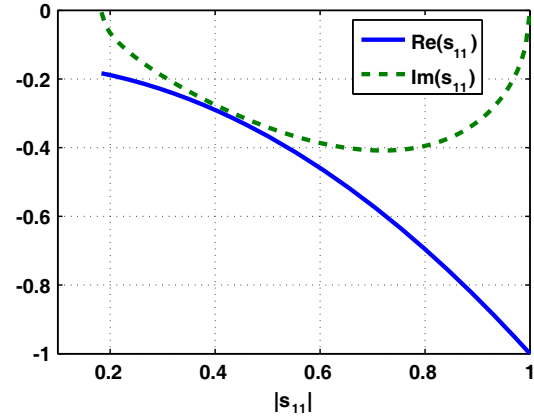**Figure 12.** The frequency variations of equivalent capacitance.

Figure 13. The variations of $\mathrm{Re}(s_{11})$ and $\mathrm{Im}(s_{11})$ versus $|s_{11}|$ for second structure.
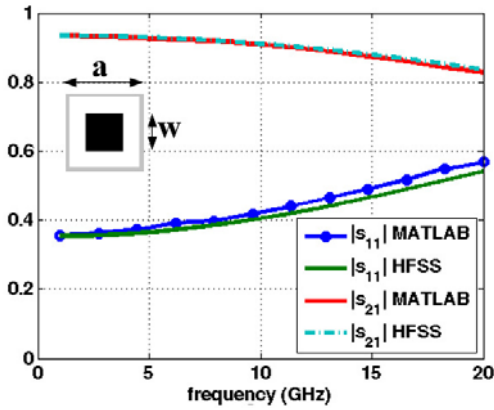

Figure 14. The frequency variations of s_{11} and s_{21} for array of square patches.
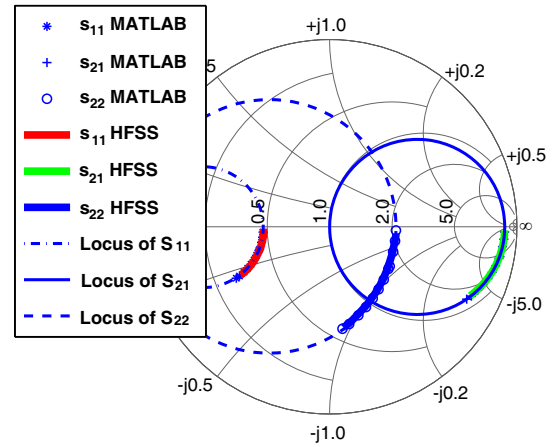

Figure 15. The frequency variations of s_{11} and s_{21} on the Smith chart.

Table 3. Physical dimensions of a metasurface made up of square patches in 2D array.

a	w	Medium I	Medium II
3 mm	2 mm	air	FR4

Table 4. Physical dimensions of a metasurface made up of square loops in 2D array.

a	l	w	Medium I	medium II
1 mm	0.565 mm	0.13 mm	air	FR4

parameters on Smith chart are plotted in Figure 18. The variations of scattering transfer parameters are demonstrated in Figure 19 for this structure.

The last structure is square perforated metal plate. A unit cell of this structure is depicted in Figure 20. Suppose that this structure is embedded in air. The geometrical properties of each element are specified in Table 5. The frequency variations of s_{11} and s_{21} for this structure are plotted in Figure 20. Figure 21 shows the variations of s-parameters for this structure on Smith chart. The variations of scattering transfer parameter corresponding to this structure are demonstrated in Figure 22. The variations of s-parameters for this metasurface is in the same way of first structure. The s_{11} for this structure goes to -1 when w increases or frequency decreases. The TEM waveguide for this structure prove this note. In zero frequency, the parallel plates are shorted by metasurface element. In contrast, increasing frequency causes that the parameter s_{11} moves to 0 along circle.

Above figures show output of MATLAB and HFSS are well-agreed with the formulas derived in the previous section.
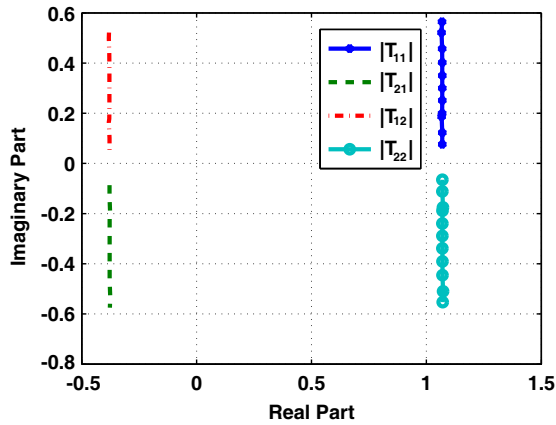

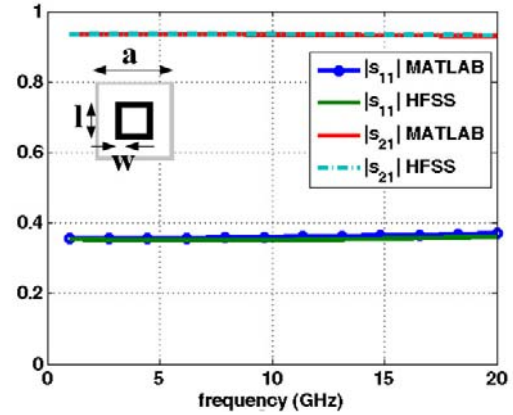**Figure 16.** The frequency variations of scattering transfer parameters.

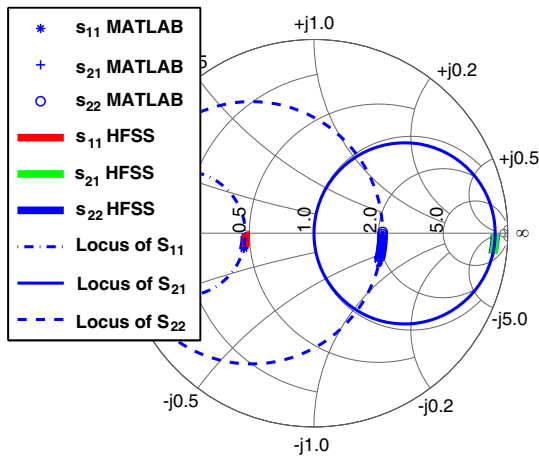**Figure 17.** The frequency variations of s_{11} and s_{21} for an array of square loops.

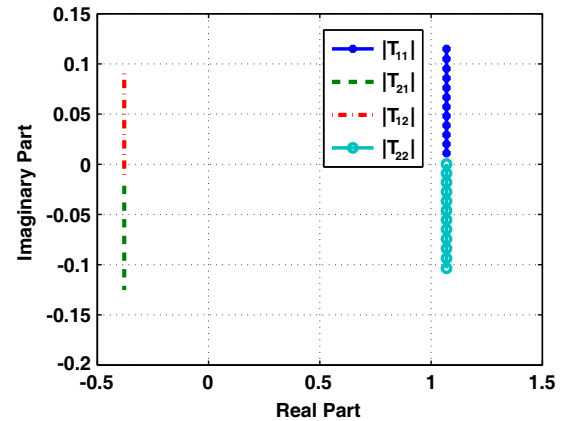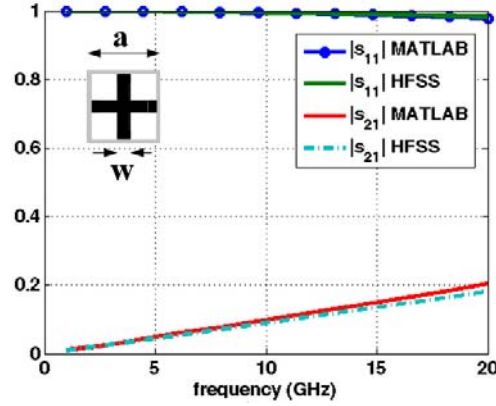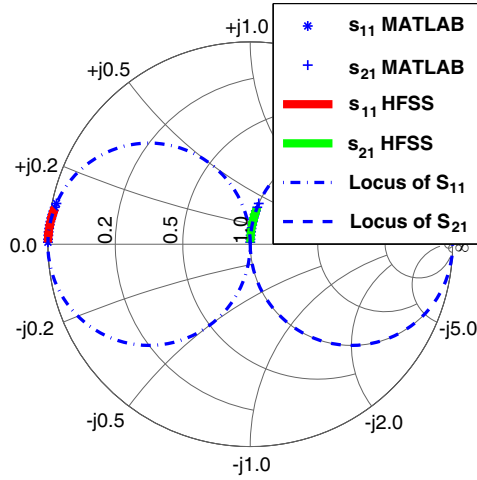**Figure 18.** The frequency variations of s_{11} and s_{21} on the Smith chart.

Figure 19. The frequency variations of scattering transfer parameters.

Table 5. Physical dimensions of a square perforated metal plate.

a	w	Medium I	Medium II
3 mm	1 mm	air	air

Figure 20. The frequency variations of s_{11} and s_{21} for square perforated metal plate.

Figure 21. The frequency variations of s_{11} and s_{21} on the Smith chart.
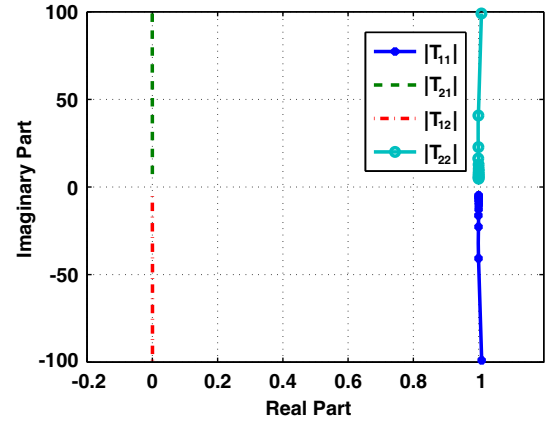
Figure 22. The scattering transfer parameters for square perforated metal plate.

4. CONCLUSION

In this paper, the behavior of a metasurface structure is considered by mode matching technique. It results in extracting new relations for predicting the behavior of metasurface structure. Regardless of physical characteristics of metasurface element, the s-parameters of metasurface are located in specific circles, which is dependent on electromagnetic properties in both sides of metasurface. It is illuminated that the metasurface element does not play any role in determining the circle. In contrast, the geometrical specifications of element are effective parameter in determining the location s-parameters on the corresponding circles. These relations are free of any limitation about the geometrical properties of metasurface element. These relations specify the variations of real and imaginary parts of reflection coefficient versus magnitude of reflection coefficient. The scattering transfer parameters are obtained in terms of scattering parameters. Simulation results prove that the new relations correctly predict the response of metasurface structure.

APPENDIX A.

The continuity of transverse electrical fields through transverse plane with the orthogonality property, established among all modes, leads to equality between total amplitude of each mode in both sides of metasurface element in the waveguide.

$$\left(\vec{E}^i + \vec{E}^r\right)_t \rightarrow \begin{cases} E_x^i + E_x^r = E_x^t \\ E_y^i + E_y^r = E_y^t \end{cases} \tag{A1}$$

For a supposed waveguide (Figure 1(b)) with considering Eq. (1), it is possible to expand all fields;

$$E_x^i + E_x^r = \sum_{m,n} \left(m\frac{\pi}{a}a_{mn} + n\frac{\pi}{b}b_{mn}\right) \varphi_{mn}(x,y) \quad E_x^t = \sum_{m,n} \left(m\frac{\pi}{a}c_{mn} + n\frac{\pi}{b}d_{mn}\right) \varphi_{mn}(x,y)$$

$$E_y^i + E_y^r = A_{00} + a_{00} + \sum_{m,n} \left(-n\frac{\pi}{b}a_{mn} + m\frac{\pi}{a}b_{mn}\right) \psi_{mn}(x,y) \tag{A2}$$

$$E_y^t = c_{00} + \sum_{m,n} \left(-n\frac{\pi}{b}c_{mn} + m\frac{\pi}{a}d_{mn}\right) \psi_{mn}(x,y)$$

Substituting these expansions into Eq. (A1);

$$E_x^r - E_x^t = 0 \rightarrow \sum_{m,n} \left(m\frac{\pi}{a}(a_{mn} - c_{mn}) + n\frac{\pi}{b}(b_{mn} - d_{mn})\right) \varphi_{mn}(x,y) = 0$$

$$\rightarrow \left\langle E_x^r - E_x^t, \varphi_{pq}(x,y) \right\rangle = \left(m\frac{\pi}{a}(a_{mn} - c_{mn}) + n\frac{\pi}{b}(b_{mn} - d_{mn})\right) \delta_{mp}\delta_{nq} \tag{A3}$$

$$E_y^i + E_y^r - E_y^t = 0 \rightarrow (A_{00} + a_{00} - c_{00}) + \sum_{m,n} \left(-n\frac{\pi}{b}(a_{mn} - c_{mn}) + m\frac{\pi}{a}(b_{mn} - d_{mn})\right) \psi_{mn}(x,y) = 0$$

$$\rightarrow \begin{cases} A_{00} + a_{00} - c_{00} = 0 \\ \left\langle E_y^i + E_y^r - E_y^t, \psi_{pq}(x,y) \right\rangle = \left(-n\frac{\pi}{b}(a_{mn} - c_{mn}) + m\frac{\pi}{a}(b_{mn} - d_{mn})\right) \delta_{mp}\delta_{nq} \end{cases} \tag{A4}$$

$$c_{00} = A_{00} + a_{00}$$
$$\begin{cases} m\frac{\pi}{a}(a_{mn} - c_{mn}) + n\frac{\pi}{b}(b_{mn} - d_{mn}) = 0 \\ -n\frac{\pi}{b}(a_{mn} - c_{mn}) + m\frac{\pi}{a}(b_{mn} - d_{mn}) = 0 \end{cases} \rightarrow \begin{cases} (a_{mn} - c_{mn}) = 0 \rightarrow c_{mn} = a_{mn} \\ (b_{mn} - d_{mn}) = 0 \rightarrow d_{mn} = b_{mn} \end{cases} \tag{A5}$$

The last relation shows that the total amplitude of each mode is equal in both sides of metasurface element.

APPENDIX B.

Since metasurface structure comprises metal elements, no power loses in structure. It means that the structure is passive,

$$|s_{21}|^2 + |s_{11}|^2 = 1 \rightarrow \frac{(\eta_0)_{\mathrm{I}}}{(\eta_0)_{\mathrm{II}}}(1 + s_{11})(1 + s_{11}^*) + |s_{11}|^2 = 1$$

$$\rightarrow 2\mathrm{Re}(s_{11}) + \left(\frac{(\eta_0)_{\mathrm{II}} + (\eta_0)_{\mathrm{I}}}{(\eta_0)_{\mathrm{I}}}\right)|s_{11}|^2 = \left(\frac{(\eta_0)_{\mathrm{II}} - (\eta_0)_{\mathrm{I}}}{(\eta_0)_{\mathrm{I}}}\right)$$

$$\rightarrow 2\frac{(\eta_0)_{\mathrm{I}}}{(\eta_0)_{\mathrm{II}} + (\eta_0)_{\mathrm{I}}}\mathrm{Re}(s_{11}) + [\mathrm{Re}(s_{11})]^2 + [\mathrm{Im}(s_{11})]^2 = \left(\frac{(\eta_0)_{\mathrm{II}} - (\eta_0)_{\mathrm{I}}}{(\eta_0)_{\mathrm{II}} + (\eta_0)_{\mathrm{I}}}\right)$$

$$\rightarrow \left\{\mathrm{Re}(s_{11}) + \frac{(\eta_0)_{\mathrm{I}}}{(\eta_0)_{\mathrm{II}} + (\eta_0)_{\mathrm{I}}}\right\}^2 + \{\mathrm{Im}(s_{11})\}^2 = \left(\frac{(\eta_0)_{\mathrm{II}}}{(\eta_0)_{\mathrm{II}} + (\eta_0)_{\mathrm{I}}}\right)^2 \tag{B1}$$

This is a circle which determines the variations of s_{11} on Smith chart.

APPENDIX C.

Following the previous appendix, the variation of $\mathrm{Re}(s_{11})$ versus $|s_{11}|$ is,

$$
2\mathrm{Re}\left(s_{11}\right) + \left(\frac{(\eta_0)_{\mathrm{II}} + (\eta_0)_{\mathrm{I}}}{(\eta_0)_{\mathrm{I}}}\right)|s_{11}|^2 = \left(\frac{(\eta_0)_{\mathrm{II}} - (\eta_0)_{\mathrm{I}}}{(\eta_0)_{\mathrm{I}}}\right)
$$

$$
\rightarrow \mathrm{Re}\left(s_{11}\right) = \frac{[(\eta_0)_{\mathrm{II}} - (\eta_0)_{\mathrm{I}}] - [(\eta_0)_{\mathrm{II}} + (\eta_0)_{\mathrm{I}}]\,|s_{11}|^2}{2(\eta_0)_{\mathrm{I}}}
$$

$$
\rightarrow \mathrm{Im}\left(s_{11}\right) = \pm\sqrt{|s_{11}|^2 - [\mathrm{Re}\left(s_{11}\right)]^2} = \pm|s_{11}|\sqrt{1 - |s_{11}|^2} \tag{C1}
$$

REFERENCES

1. Sihvola, A., "Metamaterials in electromagnetics," *Metamaterials*, Vol. 1, No. 1, 2–11, 2011.
2. Holloway, C. L., E. F. Kuester, J. A. Gordon, J. O'Hara, J. Booth, and D. R. Smith, "An overview of the theory and applications of metasurfaces: The two-dimensional equivalents of metamaterials," *IEEE Antennas and Propagation Magazine*, Vol. 54, No. 2, 10–35, 2012.
3. Watts, C. M., X. Liu, and W. J. Padilla, "Metamaterial electromagnetic wave absorbers," *Adv. Mater.*, Vol. 24, No. 1, OP98–OP120, 2012.
4. Withayachumnankul, W. and D. Abbott, "Metamaterials in the terahertz regime," *IEEE Photonics Journal*, Vol. 1, No. 2, 99–118, 2009.
5. Balanis, C. A., *Advanced Engineering Electromagnetics*, Wiley, 2011.
6. Campione, S., M. Albani, and F. Capolino, "Complex modes and near-zero permittivity in 3D arrays of plasmonic nanoshells: Loss compensation using gain," *Optical Materials Express*, Vol. 1, No. 6, 1077–1089, 2011.
7. Engheta, N., "Pursuing near-zero response," *Science*, Vol. 340, No. 6130, 286–287, 2013.
8. Pendry, J. B., D. Schurig, and D. R. Smith, "Controlling electromagnetic fields," *Science*, Vol. 312, No. 5781, 1780–1782, 2006.
9. Itoh, T., "Invited paper: Prospects for metamaterials," *Electronics Letters*, Vol. 40, No. 16, 972–973, 2004.
10. Caloz, C. and T. Itoh, "Metamaterials for high-frequency electronics," *Proceedings of the IEEE*, Vol. 93, No. 10, 1744–1752, 2005.
11. Shestopalov, V. P., "Spectral theory and excitation of open structures," *IET*, No. 42, 1996.
12. Kuester, E. F., M. A. Mohamed, M. Piket-May, and C. L. Holloway, "Averaged transition conditions for electromagnetic fields at a metafilm," *IEEE Transactions on Antennas and Propagation*, Vol. 51, No. 10, 2641–2651, 2003.
13. Holloway, C. L., M. A. Mohamed, E. F. Kuester, and A. Dienstfrey, "Reflection and transmission properties of a metafilm: With an application to a controllable surface composed of resonant particles," *IEEE Transactions on Electromagnetic Compatibility*, Vol. 47, No. 4, 853–865, 2005.
14. Marcuvitz, N., *Waveguide Handbook*, Peregrinus, Institution of Electrical Engineers, London, 1951.
15. Ulrich, R., "Far-infrared properties of metallic mesh and its complementary structure," *Infrared Physics*, Vol. 7, No. 1, 37–55, 1967.
16. Marques, R., F. Mesa, L. Jelinek, and F. Medina, "Analytical theory of extraordinary transmission through metallic diffraction screens perforated by small holes," *Opt. Express*, Vol. 17, 5571–5579, 2009.
17. Bilotti, F. and L. Sevgi, "Metamaterials: Definitions, properties, applications, and FDTD based modeling and simulation," *International Journal of RF and Microwave Computer Aided Engineering*, Vol. 22, No. 4, 422–438, 2012.
18. Huang, R., Z.-W. Li, L. B. Kong, L. Liu, and S. Matitsine, "Analysis and design of an ultra-thin metamaterial absorber," *Progress In Electromagnetics Research B*, Vol. 14, 407–429, 2009.

19. Ziolkowski, R. W., "Design, fabrication, and testing of double negative metamaterials," *IEEE Transactions on Antennas and Propagation*, Vol. 51, No. 7, 1516–1529, 2003.

20. Hsu, C. C., K. H. Lin, and H. L. Su, "Implementation of broadband isolator using metamaterial-inspired resonators and a T-shaped branch for MIMO antennas," *IEEE Transactions on Antennas and Propagation*, Vol. 59, No. 10, 3936–3939, 2011.

21. Beruete, M., I. Campillo, M. Navarro-Cia, F. Falcone, and M. Sorolla Ayza, "Molding left- or right-handed metamaterials by stacked cutoff metallic hole arrays," *IEEE Transactions on Antennas and Propagation*, Vol. 55, No. 6, 1514–1521, 2007.

22. Itoh, T., *Numerical Techniques for Microwave and Millimeter-wave Passive Structures*, Wiley, Science, 1980.

23. Pozar, D. M., *Microwave Engineering*, Wiely, 2012.

24. Collin, R. E., *Field Theory of Guided Waves*, Wiely, 1990.

25. Guglielmi, M., G. Gheri, M. Calamia, and G. Pelosi, "Rigorous multimode network numerical representation of inductive step," *IEEE Transactions on Microwave Theory and Techniques*, Vol. 42, No. 2, 317–326, 1994.

26. Widarta, A., S. Kuwano, and K. Kokubun, "Simple and accurate solutions of the scattering coefficients of E-plane junctions in rectangular waveguides," *IEEE Transactions on Microwave Theory and Techniques*, Vol. 43, No. 12, 2716–2718, 1995.

27. Wexler, A., "Solution of waveguide discontinuities by modal analysis," *Journal Title Abbreviation*, Vol. 15, No. 9, 508–517, 1967.

28. Mesa, F., R. Rodriguez-Berral, M. Garcia-Vigueras, F. Medina, and J. R. Mosig, "Simplified modal expansion to analyze frequency-selective surfaces: An equivalent circuit approach," *IEEE Transactions on Antennas and Propagation*, Vol. 64, No. 3, 1106–1111, 2016.

29. Campione, S., F. Mesa, and F. Capolino, "Magnetoinductive waves and complex modes in two-dimensional periodic arrays of split ring resonators," *IEEE Transactions on Antennas and Propagation*, Vol. 61, No. 7, 3554–3563, 2013.

30. Gonzalez, G., *Microwave Transistor Amplifiers: Analysis and Design*, Prentice Hall, 1997.

31. Conciauro, G., M. Guglielmi, and R. Sorrentino, *Advanced Modal Analysis: CAD Techniques for Waveguide Components and Filters*, John Wiley & Sons Inc., 2000.

32. Stamatopoulos, I. D. and I. D. Robertson, "Rigorous network representation of microwave components by the use of indirect mode matching," *IEEE Transactions on Microwave Theory and Techniques*, Vol. 52, No. 3, 935–944, 2004.

33. Ade, P. A., G. Pisano, C. Tucker, and S. Weaver, "A review of metal mesh filters," *Proceedings of SPIE*, Vol. 6275, 62750U–62750U, 2006.